Numerical Heat Transfer, Part A, 50: 585–606, 2006

ISSN: 1040-7782 print/1521-0634 online
DOI: 10.1080/10407780600867761

Taylor & Francis
Taylor & Francis Group

INFLUENCE OF BUOYANCY ON VORTEX SHEDDING AND HEAT TRANSFER FROM A SQUARE CYLINDER IN PROXIMITY TO A WALL

S. Bhattacharyya
Department of Mathematics, Indian Institute of Technology, Kharagpur, India

D. K. Maiti
Department of Mathematics, Birla Institute of Technology & Science, Pilani, India

S. Dhinakaran
Department of Mathematics, Indian Institute of Technology, Kharagpur, India

The flow and heat transfer past a heated cylinder of square cross section mounted horizontally above a plane wall and subjected to a uniform shear flow is considered. The flow field is considered for a moderate range of Reynolds number (based on the incident stream at the cylinder upstream face and the height of the cylinder) and Grashof number at cylinder-to-wall gap height 0.5 times the cylinder height. The flow field and heat transfer are computed through a pressure-correction-based iterative algorithm with the QUICK scheme in convective terms. The code is tested for accuracy by comparing with published results for certain values of the flow parameters. We examine the combined effects of buoyancy and shear flow on the vortex shedding behind the cylinder in close proximity to a plane wall. A boundary layer develops along the wall, and this interacts with the shear layer formed along the two sides of the cylinder. The role of the thermally induced baroclinic vorticity production term on the vortex shedding is examined. Our results show that the breakdown of vortex shedding takes place beyond certain values of Richardson number (which depends on the Reynolds number). The dependence of the average rate of heat transfer from the surface of the cylinder on Reynolds number and Grashof number is also investigated.

1. INTRODUCTION

Study of heat transfer from a protruding bluff body which is subjected to vortex shedding has several technical applications such as compact heat exchangers, cooling of electronics components, drying of various materials (textiles, veneer, paper, and film materials), cooling of glass, plastics, and industrial devices, and so on. In most cases, the range of the Reynolds number (based on the diameter of the protruding bluff body) of interest varies between l00 and 1000. For example,

Received 21 February 2005; accepted 11 March 2006.
S. Bhattacharyya wishes to thank the Department of Science and Technology, Government of India, for providing financial support through a project grant.
Address correspondence to Somnath Bhattacharyya, Department of Mathematics, Indian Institute of Technology, Kharagpur 721 302, India. E-mail: somnath@maths.iitkgp.ernet.in

NOMENCLATURE

C_L	lift coefficient
C_P	pressure coefficient $(=p^*/\frac{1}{2}\rho U^2)$
D	height of the square cylinder, m
f	frequency of vortex shedding $(=1/T)$
g	gravitational acceleration, m/s^2
Gr	Grashof number $[=g\beta_T(T_H^* - T_L^*)A^3/\nu^2]$
h	gap height from the cylinder to the plane wall, m
L	nondimensional gap height from the cylinder to the plane wall $(=h/D)$
Nu	local Nusselt number $[=(\alpha\theta/\alpha y)_{\text{lid}}]$
Nu_{av}	facewise average Nusselt number of the cylinder $\{\int_0^1 [=(\partial\theta/\partial n)]\, dl\}$
Nu_M	mean Nusselt number of the cylinder $(=1/4\Sigma_{AB} - \text{N}_{\text{u}_{\text{av}}})$
p	nondimensional pressure $(=p^*/\rho U^2)$
Pr	Prandtl number $(=\nu/\alpha)$
Re	Reynolds number $(=UD/\nu)$
Ri	Richardson number $(=\text{Gr}/\text{Re}^2)$
St	Strouhal number $(=fD/U)$
t	nondimensional time $(=t^*U/D)$
T	period of vortex shedding
u	x component of velocity, m/s
U	reference horizontal velocity, m/s
v	y component of velocity, m/s
x	horizontal distance, m
y	vertical distance, m
α	thermal diffusivity, m^2/s
β_T	coefficient of thermal expansion, K^{-1}
δ	boundary-layer thickness
θ	dimensionless temperature $[=(T^* - T_L^*)/(T_H^* - T_L^*)]$
κ	thermal conductivity, W/m s
λ	prescribed slope of the incident velocity profile
ν	kinematic viscosity coefficient, m^2/s
ρ	fluid density, kg/m

Subscripts

H	high value
L	low value
0	in the undisturbed fluid

Superscripts

*	dimensional quantity
–	time-average quantity

in analyzing the heat transfer from an electronic component in an integrated circuit (IC) with height 6 mm and air as working fluid, the Reynolds number (based on the height of the component) is 500. Within this range of Reynolds numbers, the flow can be considered as laminar. Enhancement in heat transfer from the protruding bluff body requires detailed examination of the convective transport phenomena around the body. The convective heat transfer in the region downstream is controlled by complex interactions among the boundary layer, vortex shedding, and the bluff body wake. Recently, Chung and Tucker [1] studied the unsteady heat transfer enhancement in laminar separated flows with reference to electronics cooling. There they review several relevant articles.

A numerical study of the steady-state forced-convective cooling of a horizontal printed circuit board (PCB) by flowing air under laminar flow condition has been made by Leung et al. [2]. They documented the dependence of flow and temperature fields on Reynolds number, obstacle size, and the separation between two obstacles. The forced convection from a square cylinder has been studied by Yang and Fu [3]. They found that the heat flux of the rear side of the cylinder is much less than that of the other sides. Results of Yang and Fu [3] show that the heat flux for the case of flow with vortex shedding is higher than that without vortex shedding.

Noto and Matsumoto [4, 5] did a series of studies on the development of the vortex cores in a Karman vortex street behind a heated cylinder placed in a vertically upward free stream. They reported that the vortex shedding frequency increases with increasing cylinder temperature. However, above a critical heat input, vortex

shedding is suppressed. Input of heat causes these vortices to disappear, resulting in a thermal plume. Chang and Sa [6] examined the buoyancy effect on vortex shedding in the near-wake of a heated/cooled circular cylinder in vertical free stream. They found that Nusselt number increases monotonically with the Grashof number when the flow is steady with twin vortices and breakdown of vortex shedding by the heating effect. Hatanaka and Kawahara [7] investigated the flow behavior behind a heated/cooled circular cylinder to find a critical value of Richardson number, at which flow changes from a periodic to a twin vortex pattern for Reynolds number 100. The effect of the angle between the main flow direction and the gravitational vector was investigated numerically by Noto [8]. He found that the angle of attack has a major influence on the vortex street characteristics. From this study it was found that for angle of attack smaller than 90° the natural frequency becomes even greater than for the unheated situation.

The wake structure behind a heated horizontal circular cylinder in nonvertical cross-flow has been considered by Kieft et al. [9]. They investigated the variation of Richardson number at a fixed Reynolds number and found a downward motion of the shed vortices. Recently, Ren et al. [10] performed an experimental and numerical study of the vortex formation process behind a heated cylinder exposed to a horizontal stream.

When the cylinder is placed in proximity to a solid wall, the strength of the upper and lower shear layers separated from the surfaces of the cylinder is not equal, and the vortex shedding pattern is distorted. Practical examples where this type of flow is observed include wind flow across free-spanning structures and buildings and forced-air cooling of board-mounted electronic components. The form of the wake and the vortex shedding behind a cylinder in proximity to a wall or when the cylinder is exposed to a shear flow has been studied by several authors, including Kiya et al. [11], Bearman and Zdravkovich [12], Bosch and Rodi [13], Lei et al. [14], Zovatto and Pedrizzetti [15], and Bailey et al. [16]. It has been found that the presence of shear in the flow has the effect of delaying vortex shedding.

Flow and heat transfer characteristics of a rectangular cylinder exposed to a uniform flow with ground effect has been studied by Shuja et al. [17]. They considered laminar flow and varied the gap height from 1.0 to 5.0. The forced convection from a square cylinder placed symmetrically in a channel was studied by Sharma et al. [18]. Rosales et al. [19] considered the forced convection from a pair of cylinders placed at various gap heights.

From the above discussion, it is clear that most of the previous experimental and numerical studies on vortex shedding from a heated cylinder in cross-flow considered either the cylinder placed in a unbounded domain or the cylinder placed symmetrically within a channel. Wall proximity with nonuniform incident flow has not been addressed previously. The presence of shear in the flow and the wall confinement produces an asymmetry in the two separated shear layers emerging from the upper and lower faces of the cylinder. Our objective is to investigate the effect of the input of heat on the interaction of the separated shear layers. Vortex shedding in the mixed-convection regime is physically more complicated owing to the buoyancy effect added to the viscous phenomena. Several studies have been done on steady-state mixed convection with the Reynolds number limited up to 40 (Badr [20]). Our specific concern is with the case of a heated bluff body so close to the flat

surface that the far field may be viewed as uniform shear flow. The cylinder-to-wall gap height is taken to be 0.5 times the cylinder height for a range of Reynolds number (100–250) with Grashof number $0–10^5$. In order to investigate the influence of buoyancy on vortex shedding and heat transfer from the heated cylinder, we considered cylinder-to-wall gap height 0.5 times the cylinder height, since a regular vortex shedding occurs at this gap height. The governing equations of the flow and energy transport are solved numerically through the finite-volume method with a pressure-correction-based iteration algorithm. The flow and heat transfer characteristics due to the ground effect are presented in terms of nondimensional quantities. Our results show that the addition of heat to the cylinder may lead to a breakdown of vortex shedding, resulting in the wake becoming steady.

The configuration and governing equations are described in the next section. Section 3 presents an outline of the numerical method used in this study. In Section 4, the numerical results for the flow and heat transfer characteristics are presented and discussed for different values of Reynolds number, Grashof number (and hence for different values of Richardson number), and for fixed value of cylinder-to-wall gap height 0.5 times the cylinder height. Conclusions and further comments are provided in Section 5.

2. FORMULATION

We consider a plane wall lying along the x axis and a long cylinder of square cross section of height D, placed parallel to the plane wall at a height h from the plane wall (see Figure 1). The cylinder is so close to the wall that the wall appears indefinitely long (the x axis) and the fluid appears to be of semi-infinite extent normally, with uniform incident shear flow. We take the prescribed slope λ of the incident velocity profile at the surface multiplied by D, that is, $U = \lambda D$, as the velocity scale and the height of the cylinder D as characteristic length. The cylinder is kept at a constant temperature T_H^*, while the plane wall is at a constant temperature T_L^*. The ambient stream has a uniform temperature T_L^*, with $T_L^* < T_H^*$.

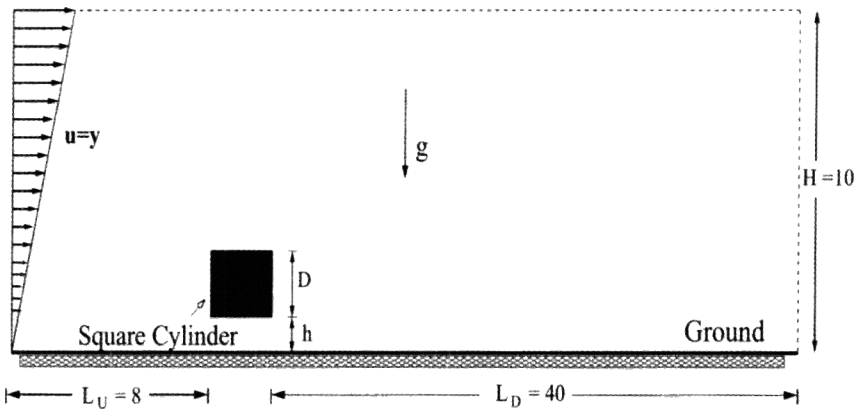

Figure 1. Schematic of the computational domain for the shear flow past a square cylinder placed near the ground.

The nondimensional Navier-Stokes equations with the energy equation governing the flow and heat transfer characteristics are given by

$$\frac{\partial u}{\partial x}+\frac{\partial v}{\partial y}=0 \tag{1}$$

$$\frac{\partial u}{\partial t}+\frac{\partial u^2}{\partial x}+\frac{\partial (uv)}{\partial y}=-\frac{\partial p}{\partial x}+\frac{1}{\mathrm{Re}}\left(\frac{\partial^2 u}{\partial x^2}+\frac{\partial^2 u}{\partial y^2}\right) \tag{2}$$

$$\frac{\partial v}{\partial t}+\frac{\partial (uv)}{\partial x}+\frac{\partial v^2}{\partial y}=-\frac{\partial p}{\partial y}+\frac{1}{\mathrm{Re}}\left(\frac{\partial^2 v}{\partial x^2}+\frac{\partial^2 v}{\partial y^2}\right)+\theta\,\mathrm{Ri} \tag{3}$$

$$\frac{\partial \theta}{\partial t}+\frac{\partial (u\theta)}{\partial x}+\frac{\partial (v\theta)}{\partial y}=\frac{1}{\mathrm{Re}\,\mathrm{Pr}}\left(\frac{\partial^2 \theta}{\partial x^2}+\frac{\partial^2 \theta}{\partial y^2}\right) \tag{4}$$

The nondimensional variables are defined as

$$\begin{aligned} u&=\frac{u^*}{U} \qquad v=\frac{v^*}{U} \qquad p=\frac{p^*}{\rho U^2} \qquad \theta=\frac{T^*-T_L^*}{T_H^*-T_L^*} \\ x&=\frac{x^*}{D} \qquad y=\frac{y^*}{D} \qquad t=\frac{t^* U}{D} \end{aligned} \tag{5}$$

The variables with superscript * denote dimensional variables. In writing the above equations, the usual Boussinesq approximation of neglecting the density variation (due to heating) in all terms except the buoyancy force term [represented by the last term in Eq. (3)] is made.

At the far upstream, the transverse velocity component is set to zero, and a sheared profile for the longitudinal velocity component is assumed, which is in accord with the boundary-layer theory. At the plane wall and cylinder surface, no-slip boundary conditions are applied. The cylinder is assumed to be heated with uniform temperature.

$$u=v=0, \quad \theta=1 \qquad \text{on the cylinder surface} \tag{6}$$

$$u=v=0, \quad \theta=0 \qquad \text{on the plane wall } y=0 \tag{7}$$

Further,

$$u\longrightarrow y, \quad v\longrightarrow 0, \quad \theta\longrightarrow 0 \qquad \text{in the upstream} \tag{8}$$

A zero-gradient boundary condition is applied at the outflow boundary, and a symmetry boundary condition is prescribed on the top lateral boundary.

The vorticity component, ω, perpendicular to the plane is given by

$$\omega = \frac{\partial v}{\partial x} - \frac{\partial u}{\partial y}$$

The vorticity transport equation can be expressed as

$$\frac{\partial \omega}{\partial t} + (u, v) \cdot \nabla \omega = \frac{1}{\mathrm{Re}} \nabla^2 \omega + \mathrm{Ri} \frac{\partial \theta}{\partial x} \tag{9}$$

The second term on the right-hand side of (9) is the thermally induced baroclinic production term, representing the production of vorticity within the flow domain due to temperature gradients perpendicular to **g** (Steenhoven et al. [21]).

3. NUMERICAL METHOD

The computational domain is divided into Cartesian cells. A staggered grid arrangement is used in which the velocity components are stored at the midpoints of the cell sides to which they are normal. The pressure and temperature are stored at the center of the cell. A pressure-correction-based iterative algorithm is employed for solving the governing equations. This method involves integration of the continuity, momentum, and energy equations over a two-dimensional control volume on a staggered grid system. A third-order-accurate QUICK (Quadratic Upstream Interpolation for Convective Kinematics, Leonard [22]) is employed to discretize the convective terms in the Navier-Stokes equations. An implicit first-order scheme is used to discretize the time derivatives present.

The u-momentum equation after integration over the u-control volume (Figure 2*a*) becomes

$$F_e u_e - F_w u_w + F_n u_n - F_s u_s = b \tag{10}$$

where F_e is the nonlinear coefficient of u_e and b contains the source terms, diffusion terms, and time-derivative terms. The convective term at any interface is estimated by a quadratic interpolation of u. For example, at the east face (Figure 2*b*), we have

$$u_e = \left(\frac{3}{8}u_E + \frac{3}{4}u_P - \frac{1}{8}u_W\right) \qquad \text{if } F_e > 0$$

$$u_e = \left(\frac{3}{4}u_E + \frac{3}{8}u_P - \frac{1}{8}u_{EE}\right) \qquad \text{if } F_e < 0$$

which can be summarized as

$$F_e u_e = \left(\frac{3}{8}u_E + \frac{3}{4}u_P - \frac{1}{8}u_W\right)[[F_e, 0]] - \left(\frac{3}{4}u_E + \frac{3}{8}u_P - \frac{1}{8}u_{EE}\right)[[-F_e, 0]] \tag{11}$$

The v-momentum equation is discretized in the similar manner.

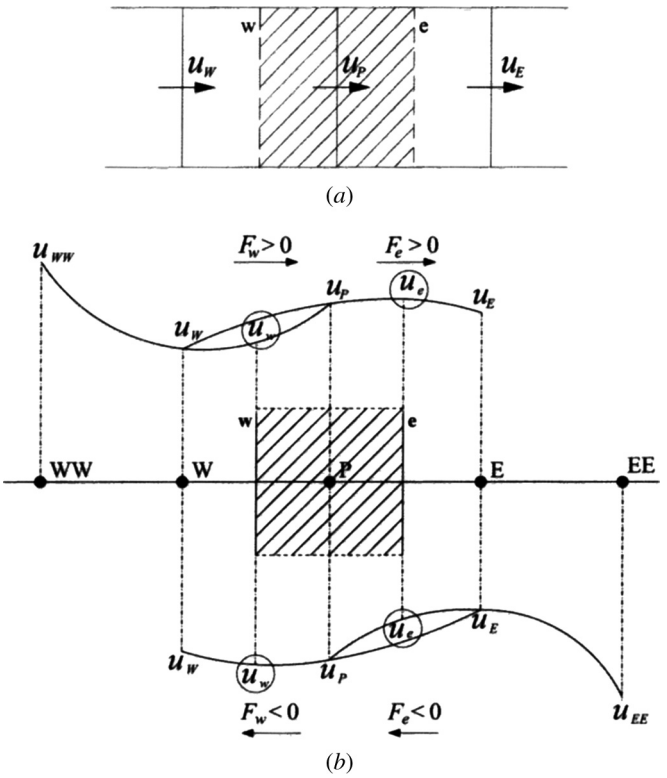

Figure 2. Shematic of (*a*) *u*-control volume and (*b*) quadratic upstream-based interpolation for *u*.

Thus, at any time step, a single iteration in this algorithm consists of the following sequential steps.

1. Implicit calculations of the momentum and energy equations are performed. The equations are discretized through the scheme as discussed above. Due to coupling of the energy equation with the momentum equations, we solve the system of algebraic equations through a block elimination method.
2. The Poisson equation for pressure correction is solved using the successive under-relaxation method.
3. The velocity field at each cell is updated using the pressure correction.

Iteration at each time step is continued until the divergence-free velocity field is obtained. However, for this purpose, the divergence in each cell is towed below a pre-assigned small quantity (ϵ). In the present case, ϵ is 0.5×10^{-4}.

A time-dependent numerical solution is achieved by advancing the flow field variables through a sequence of short time steps of duration δt. At the initial stage of motion the time step δt is taken to be 0.001, which is subsequently increased to 0.005 after the transient state.

3.1. Grid Consideration and Algorithm Testing

The height of the top lateral boundary and the outflow boundary are chosen large enough so that the influence of the boundary conditions on the wall shear stress is very weak. Tests were made in order to determine the suitable distances of the top boundary and downstream boundary. The outflow boundary distances are increased with an increase of Reynolds number. For a typical computation at $\mathrm{Re} = 250$, for example, the top lateral boundary and the outflow boundary are taken as $10\,D$ from the plane wall and $40\,D$ from the cylinder rear face, respectively. Further changes on outflow boundary and top lateral boundary distances do not produce any significant changes in the results.

A nonuniform grid distribution in the computational domain is incorporated. Figure 3 shows the grid distribution near the cylinder faces and the plane wall. The grid is finer near the surfaces of the square cylinder and the wall, to better resolve the gradients near the solid surfaces. To check the grid independence we performed computations for four sets of grids, 338×210, 676×420, 338×210, and 169×105 with the first and second number being the number of mesh points in the x direction and in the y direction, respectively. The maximum distance of the first grid point from each wall is $0.01\,A$, and it is $0.005\,A$ for the coarse and fine grids, respectively. The effect of grid size on Strouhal number (St) and the time-average drag coefficient ($\overline{C}_D$) experienced by the cylinder at various values of Richardson number ($\mathrm{Ri} = 0$–1.5) at $\mathrm{Re} = 250$ for shear flow past a square cylinder placed near the ground is presented in Figures 4 and 5. The computed average drag coefficient and Strouhal number are almost identical at grid size 338×210 and 676×420, with the changes occuring in the second and third decimal places in $\overline{C}_D$ and St, respectively. The maximum percent differences in $\overline{C}_D$ and St are found to be 0.31% and 0.27% for the 338×210 and 676×420 grids, respectively. Halving the grids from 338×210 to 169×105 produces maximum percent differences of 2.86% and 1.53% in $\overline{C}_D$ and St, respectively. The grid that best captures the flow field with the least computational time has been found to be 338×210 and hence is used for all the calculations performed in this study.

In order to assess the accuracy of our numerical method, we have computed the Strouhal number and the average drag coefficient for uniform flow past a square cylinder in an unbounded domain at different values Re and compared with the results due to Davis and Moore [23], Franke et al. [24], Arnal et al. [25], and Hwang

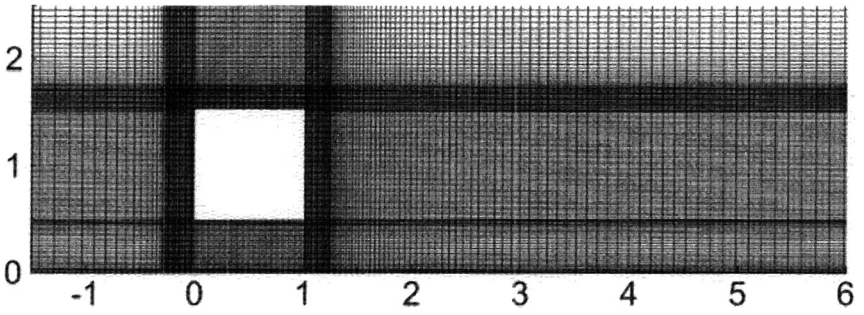

Figure 3. Nonuniform grid distribution in the vicinity of the cylinder and the ground.

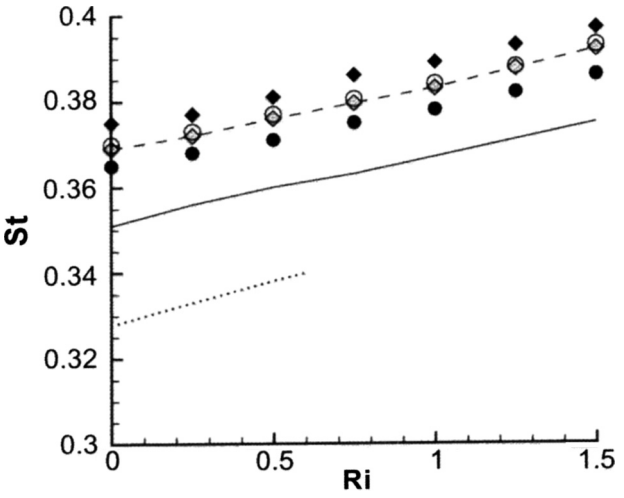

Figure 4. Variation of St with Ri at Re = 125, 200, and 250.

and Yao [26]. Our results are in excellent agreement with all of these. For the sake of brevity, the results are not presented here.

We computed the Strouhal number, average drag coefficient, and the surface-averaged Nusselt number ($\overline{\mathrm{Nu}}_M$) for the case of forced convection past a cylinder placed symmetrically within a channel and compared the results with those of Sharma et al. [18]. Our results are found to be in excellent agreement with those of Sharma (Figures 6*a*–6*c*).

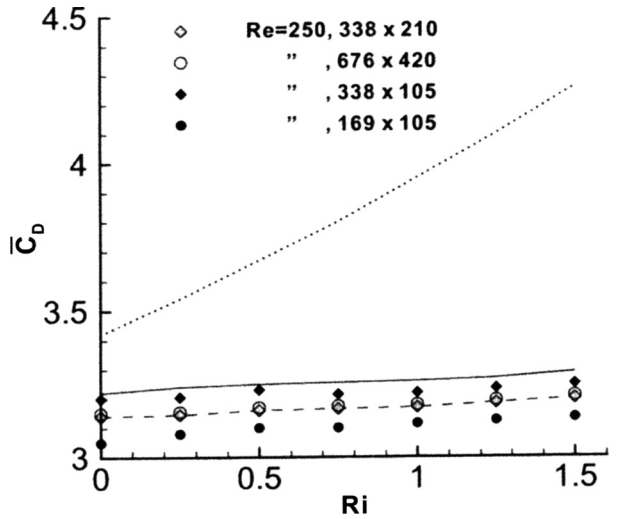

Figure 5. Variation of average drag coefficient with Ri at Re = 125, 200, and 250. Grid size effect at Re = 250 is also included in Figures 4 and 5. Dotted line, Re = 125; solid line, Re = 200; dashed line, Re = 250.

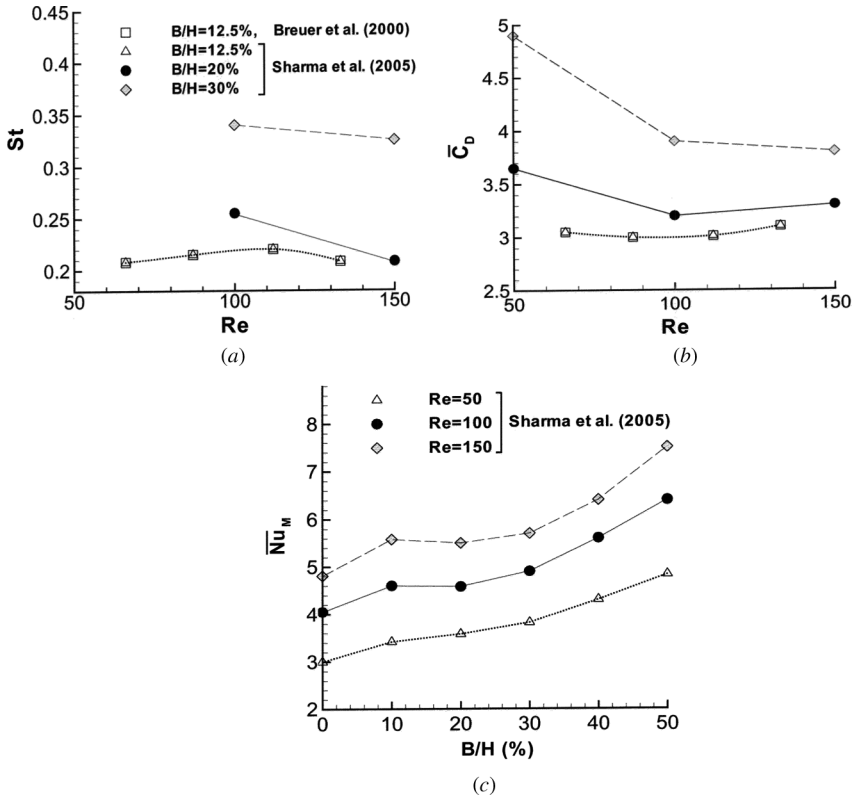

Figure 6. Comparison of (*a*) Strouhal number, (*b*) average drag coefficient, and (*c*) mean Nusselt number for different blockage ratios ($B/H\%$) at $\mathrm{Re} = 125$ (dotted line), $\mathrm{Re} = 200$ (solid line), and $\mathrm{Re} = 250$ (dashed line) for the confined forced-convective flow past a square cylinder in a channel. The legend in (*a*) is also applicable to (*b*).

A comparison of our computed results (St and $\overline{C}_D$) when the cylinder of height D is placed in a boundary layer of thickness δ at a gap-height ratio L from a wall has also been compared with those of Hwang and Yao [26], The boundary-layer flow is generated from a uniform stream over a flat plate. Table 1 displays the comparison for various values of δ/D and $L = h/D$ at $\mathrm{Re} = 1{,}000$. Our results are in excellent agreement with the results of Hwang and Yao [26].

All the numerical calculations were performed on a Sun Fire V250 server powered by a 1.28-GHz UltraSPARC IIIi processor. A typical calculation at $\mathrm{Re} = 250$ took a maximum CPU time of 6 h for a nondimensional time $t = 100$.

4. RESULTS AND DISCUSSION

The present flow field is governed by three parameters: the Reynolds number Re, the cylinder-to-wall gap height L, and the Grashof number Gr. The Richardson number, $\mathrm{Ri} = \mathrm{Gr}/\mathrm{Re}^2$, measures the relative importance of buoyancy-driven natural convection to the forced convection. We have presented the numerical solutions at

Table 1. Comparison of Strouhal number and time-averaged drag coefficient at Re = 1,000 and for boundary-layer thickness $\delta/D = 0.8$, 5.0 at various gap heights L

Configuration		Strouhal number (St)			Drag coefficient ($\overline{C}_D$)		
δ/D	L	Present	Hwang et al. [27]	Percent error	Present	Hwang et al. [27]	Percent error
0.8	5.5	0.121	0.122	1.64	1.99	1.98	0.50
	3.5	0.121	0.124	2.41	1.97	1.97	0.00
	1.5	0.132	0.135	2.22	2.13	2.14	0.46
	1.0	0.144	0.140	2.86	2.10	2.15	2.36
5.0	5.5	0.122	0.121	0.82	1.97	1.94	1.54
	3.5	0.106	0.111	4.50	1.64	1.66	1.21
	1.5	0.086	0.088	2.27	0.80	0.79	1.26
	1.0	0.083	0.080	3.75	0.52	0.50	4.00

$L = 0.5$ for Richardson number in the range $0 \leq \mathrm{Ri} \leq 1.6$ at Reynolds numbers Re = 100, 125, 200, and 250 and hence for different values of Grashof number number ($0 \leq \mathrm{Gr} \leq 10^5$).

The critical Reynolds number for the onset of vortex shedding at different Grashof numbers is presented in Figure 7. The heat input to the cylinder causes a delay in vortex shedding and this critical value of Re increases monotonically with Gr when $\mathrm{Gr} > 10^3$. Heating the cylinder causes a stabilization effect in the shear layer issuing from the lower side of the cylinder, and the fluid near the cylinder moves in the upward direction. For Gr = 0 (nonbuoyancy case), a steady wake results for Reynolds number up to 100, and the wake is periodic at Re = 125. For $\mathrm{Gr} = 10^4$, we find that the wake is steady even at Re = 125. At higher Richardson number Ri = 1.6, with $\mathrm{Gr} = 10^5$, a steady wake is observed for Reynolds number up to Re = 250.

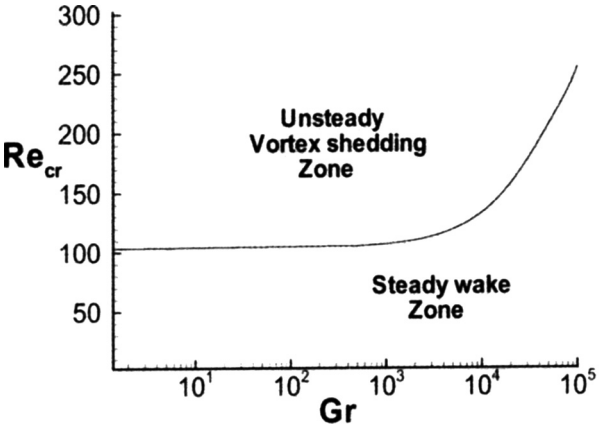

Figure 7. Critical Reynolds number (Re_{cr}) for the onset of vortex shedding as a function of Grashof number.

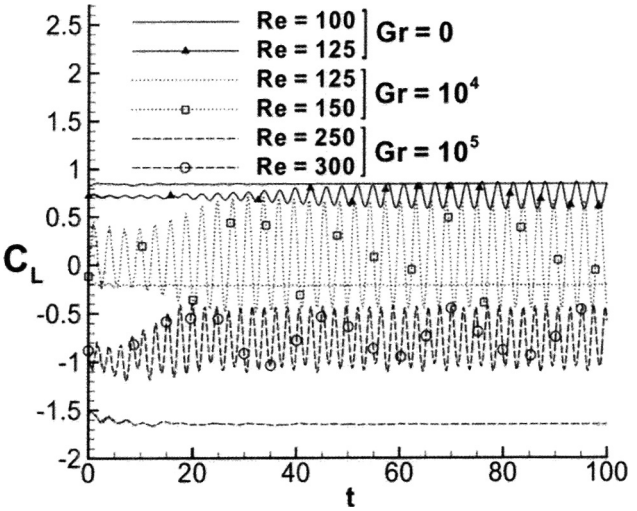

Figure 8. Time evolution of lift coefficient at various Gr and Re. Gr = 0, Re = 100, 125; Gr = 10^4, Re = 125, 150, and Gr = 10^5, Re = 250, 300.

By increasing the Reynolds number ($\mathrm{Re} \geq 150$) with fixed Grashof number ($\mathrm{Gr} = 10^4$), the wake becomes unsteady and after a transition flow reaches a periodic state. Time evolution of the lift coefficient (C_L) on the cylinder is presented in Figure 8 for different values Re (=100, 125, 150, 250, and 300) when the gap height is 0.5 for Gr = 0, 10^4, and 10^5.

The variation of Strouhal number with the Richardson number is shown in Figure 4. The shedding frequency increases monotonically with the Richardson number. As Richardson number increases for fixed Reynolds number, the wall shear layer along the surface of the cylinder is accelerated, which results in an increment in Strouhal number. Our results show that the periodic vortex shedding behind the cylinder disappears beyond a critical value of Richardson number for a fixed Reynolds number. Beyond this critical Ri, which depends on Re, the flow becomes steady, with twin vortices appearing behind the cylinder. The form of the steady wake will be described later. We find that the vortex shedding suppression occurs for $\mathrm{Ri} > 0.6$ at Re = 125. This critical value of Ri increases as Re increased. This process has been observed experimentally by Noto and Matsumoto [4] for a circular cylinder placed in an upward stream in an unbounded fluid. They referred to this phenomenon as the "breakdown of the Karman vortex street."

Figures 9*a*–9*d* display the evolution of instantaneous vorticity during a cycle of vortex shedding when Re = 250 and $L = 0.5$ with $\mathrm{Gr} = 10^4$ (i.e., Ri = 0.16). The development of the wake displayed in the figures is no longer symmetric. In the vicinity of the cylinder and the plane wall, there are three separated shear layers. A separated shear layer of negative vorticity develops along the upper face of the cylinder and a shear layer of positive vorticity develops along the bottom face of the cylinder. The shear layer that develops along the plane wall has negative vorticity. The formation and suppression of the vortex shedding results from the interaction of these

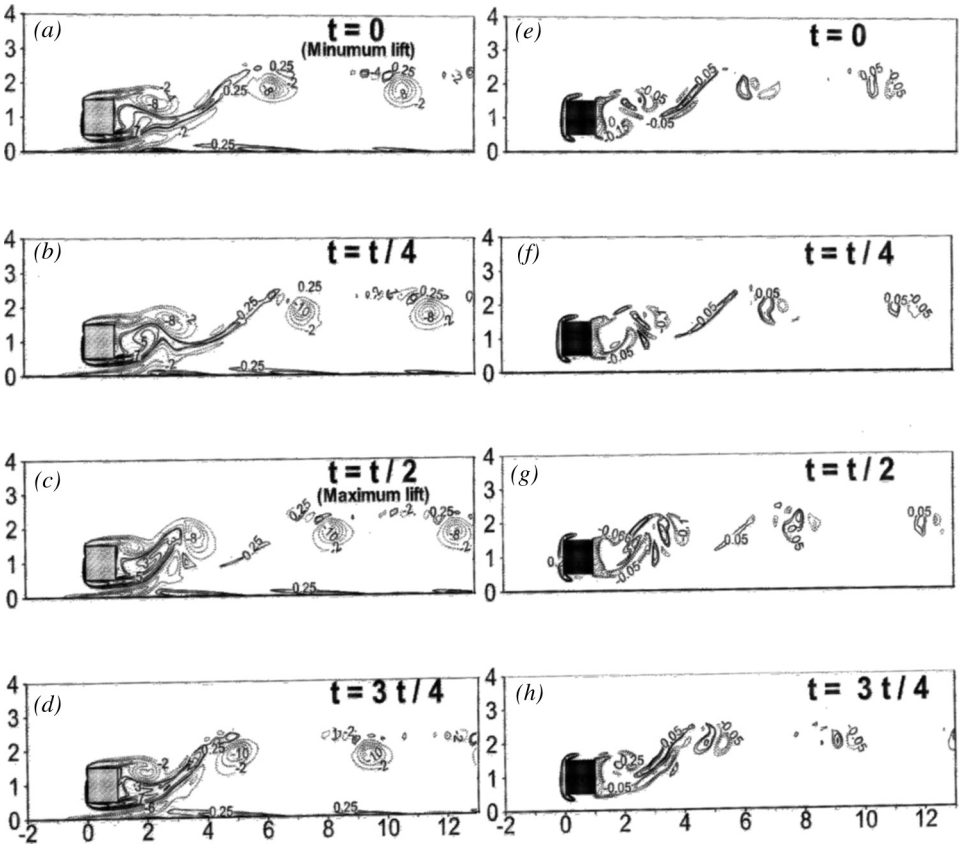

Figure 9. Time evolution of vorticity (*a–d*) and vorticity production (*e–h*) during a shedding cycle at Re = 250 and Ri = 0.16 (Gr = 10^4).

three shear layers. At the starting of the shedding cycle $t = 79.54$ ($t = 0$, say), where the cylinder experiences the maximum drag (minimum lift), the positive vortex induced by the lower shear layer grows rapidly before being shed. A small, weaker positive vortex is shed into the wake at $t = 80.178$ ($t = T/4$). This positive vortex is pushed downward by the upper layer, induced strong negative vortex. At time $t = 80.835$ ($t = T/2$), the negative vortex on the upper face of the cylinder grows rapidly. A strong, nearly circular negative vortex sheds from the upper shear layer during the shedding cycle where the lift is near maximum. In the wake, the negative vortex originates from the upper shear layer, which moves almost along the horizontal direction. The wall shear layer (boundary layer) on the wall in the downstream of the cylinder with negative vortex cancels part of the positive vorticity induced by the lower shear layer of the cylinder, which weakens the lower shear layer. Thus a weak positive vortex shedding occurs behind the cylinder. Figures 9*a*–9*d* show that as the cylinder lower face induced positive shear layer grows, the boundary layer along the wall thickens. Downstream of the cylinder, vortex-induced separation from the wall occurs and an induced secondary vortex forms along the wall. This separation from

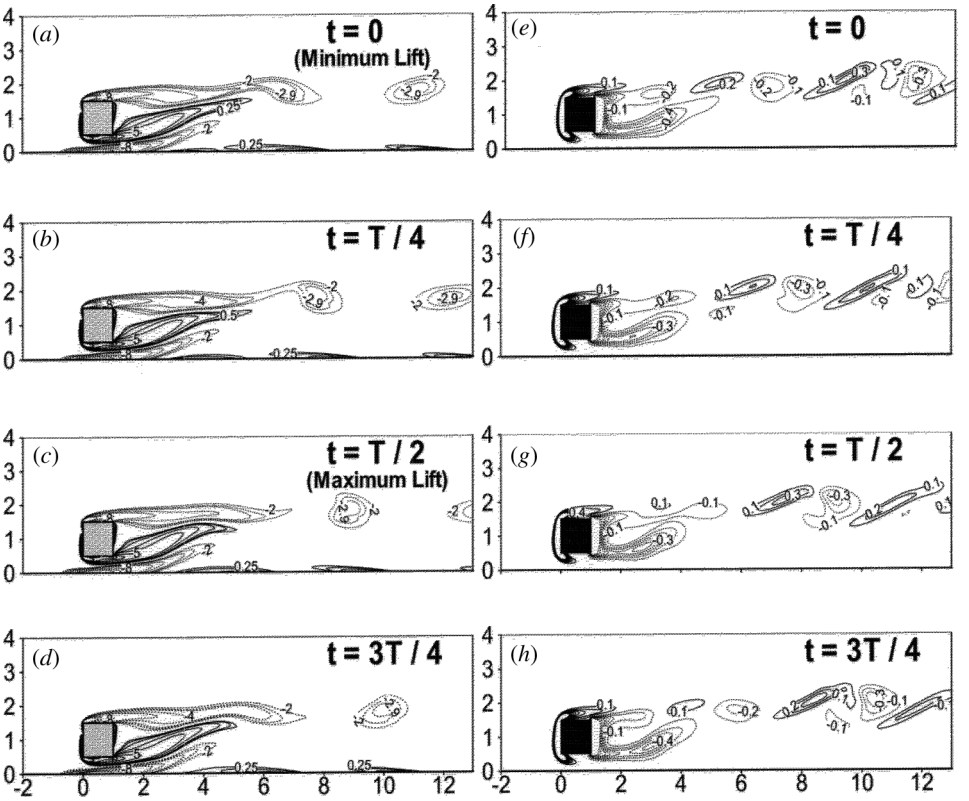

Figure 10. Time evolution of vorticity (*a–d*) and vorticity production (*e–h*) during a shedding cycle at Re = 125 and Ri = 0.5.

the wall appears to be coupled in a periodic manner with vortex shedding from the cylinder.

The instantaneous vorticity contours during a shedding cycle at higher Ri (= 0.5) with Re = 125 are presented in Figures 10*a*–10*d*. The results show that the separated lower shear layer reattaches to the cylinder surface itself, without rolling up. The magnitude of vorticty in the upper shear layer is increased. At higher Ri, a strong upward motion occurs in the near-wake. This upward flow enhances the formation of the upper vortices and induces a thermal plume in the near-wake, which can be observed in Figures 11*e*–11*h*.

The instantaneous vorticity production due to baroclinic production during a shedding cycle is shown in Figures 9*e*–9*h* for Re = 250, Ri = 0.16. The corresponding distribution of baroclinic production for Ri = 0.5 and Re = 125 is shown in Figures l0*e*–10*h*. The baroclinic production term ($\mathrm{Ri}\,\partial\theta/\partial x$) is positive along the upstream side of the cylinder, but negative in the downstream side. The negative baro-clinic production strengthen the negative shear layer and reduces the strength of the positive shear layer emerging from the cylinder. In the wake, a closed area of negative and positive production is observed. The zone of positive production appears just upstream of the zone of negative production. Thus the net contribution

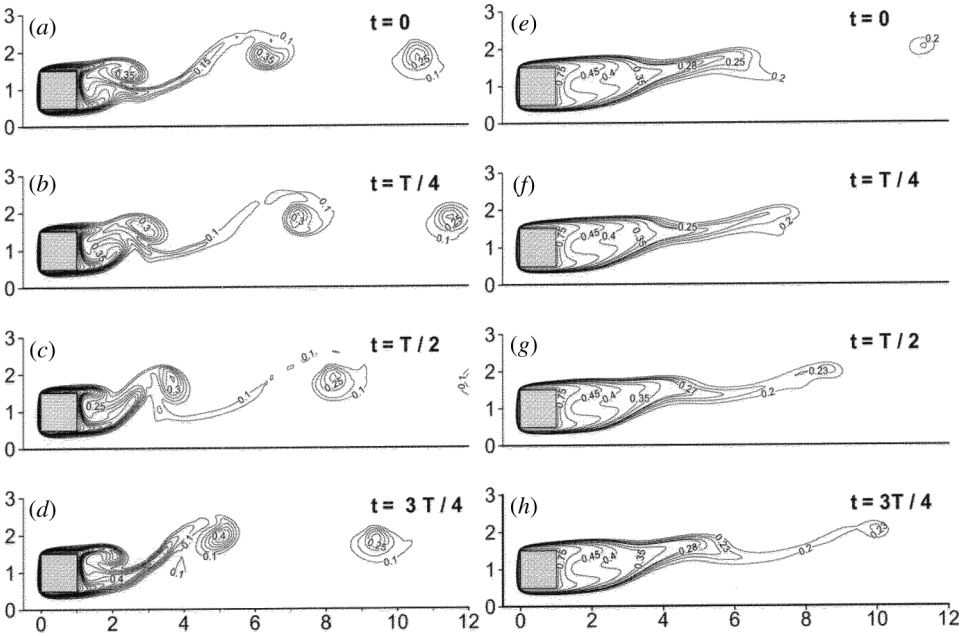

Figure 11. Isotherms during a shedding cycle: (*a–d*) Re = 250 at Ri = 0.16 (Gr = 10^4); (*e–h*) Re = 125 at Ri = 0.5.

of the baroclinic vorticity production in the far downstream of the cylinder is not significant. It is clear from the figures that buoyancy produces further asymmetry in the shear layer emerging from the two sides of the cylinder surface. We find, by comparing Figures 9*e*–9*h* and Figures 10*e*–10*h*, that at higher Ri, the magnitude of the production is large.

The instantaneous temperature field is presented at different time levels during a vortex shedding cycle in Figures 11*a*–11*d* at Re = 250 for gap height $L = 0.5$ with Grashof number Gr = 10^4. As both vorticity and thermal energy are being transported by the flow in the wake, the contour lines of vorticity and temperature have similar features. The plots of the temperature distribution show that heat is distributed within the flow field as isolated warm blobs. These warm blobs are captured within the vortex structures and advected downstream without being influenced too much by mixing with their surroundings. The thermal boundary-layer growth starts almost symmetrically from the front face of the cylinder and becomes thicker toward the rear. At higher Richardson number (Ri = 0.5) at Re = 125, the instantaneous temperature field shows (Figures 11*e*–11*h*) that a thermal plume in the horizontal direction arises in the near-wake of the cylinder. In the plume, the warm fluid lies below the cold one.

Figures 12*a*–12*e* and Figures 12*f*–12*j* show the effect of the rise of cylinder surface temperature on the instantaneous flow and thermal field. The result are shown for Re = 125 at various Ri (=0, 0.5, 0.75, 1.0, 1.5). The instantaneous temperature field in the near-wake is shown in Figures 12*f*–12*j*. It may be noted that vortex shedding occurs for $0 \leq \mathrm{Ri} < 0.6$ at Re = 125, but the regular vortex shedding is

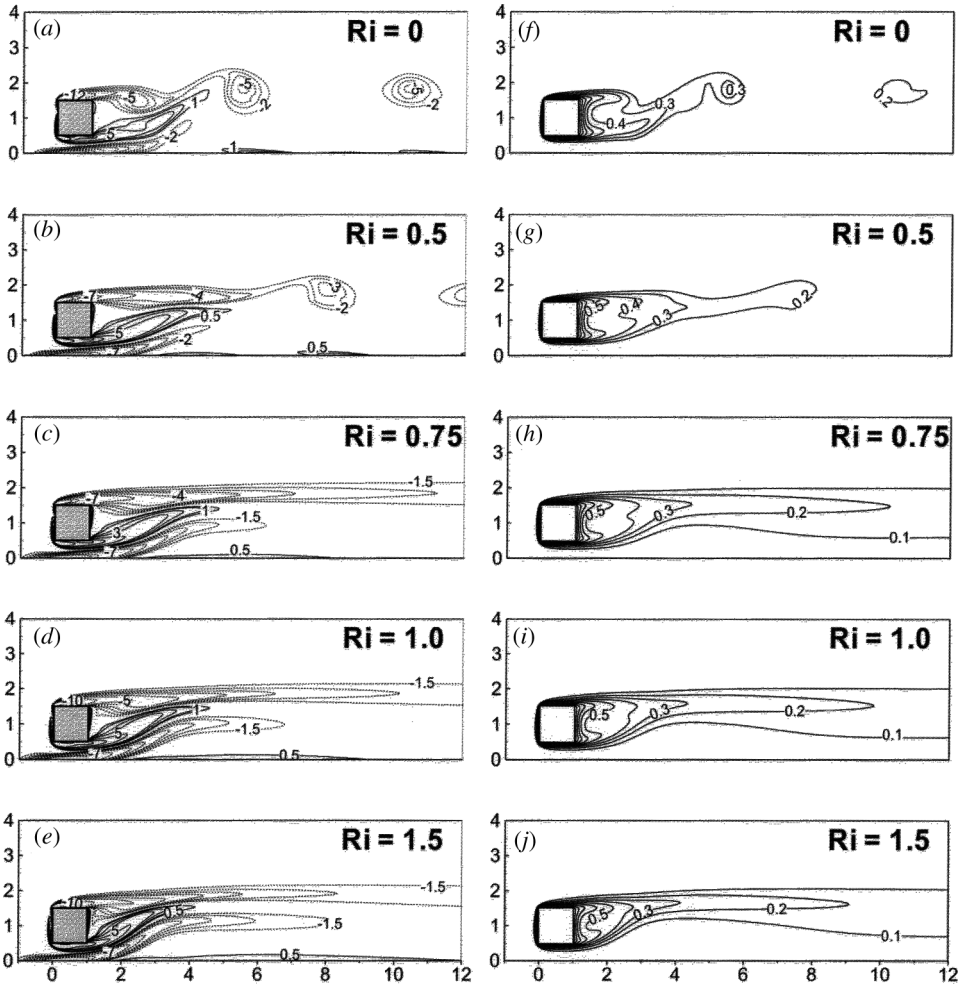

Figure 12. Instantaneous vorticity lines (*a–e*) and isotherms (*f–j*) for the cylinder placed near the ground at Re = 125 for various Richardson numbers: (*a*, *f*) Ri = 0 (unsteady); (*b*, *g*) Ri = 0.5 (unsteady); (*c*, *h*) Ri = 0.75 (steady); (*d*, *i*) Ri = 1.0 (steady); (*e*, *j*) Ri = 1.5 (steady).

suppressed for Ri = 0.75, 1, and 1.5. Our results show that the horizontal thermal plume extends to a large distance downstream of the cylinder for higher values Ri.

We have seen that upon increasing the Richardson number from Ri = 0.0 (i.e., Gr = 0) with Re = 125, the periodic vortex shedding behind the cylinder disappears and the wake becomes steady for Ri > 0.6. The form of the wake beyond this critical value of Ri is presented in Figures 12*c*–12*e* for Re = 125 at Ri = 0.75, 1.0, and 1.5 (Gr = 11,718, 15,625, 23,437). The wake consists of twin vortices of opposite sign attached to the rear of the cylinder faces. For a fixed Reynolds number, the increment in Richardson number is due to the increase of cylinder surface temperature. As suggested by Gerrard [27] for flow past a circular cylinder, for vortices to shed, the wake cavity should open and form instantaneous "alleyways" for fluid

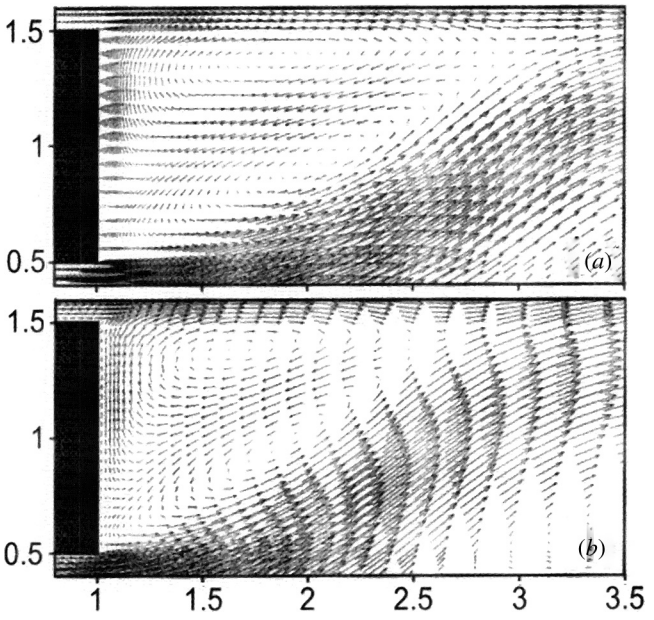

Figure 13. Velocity vectors downstream the cylinder for Re = 125 at (*a*) Ri = 1; (*b*) Ri = 1.5.

to penetrate the cavity. For the case of a heated cylinder, the entrainment of the ambient cold fluid into the wake diminishes and eventually vanishes at this critical value of Richardson number. This leads to suppression of vortex shedding beyond the critical Richardson number. The strong upward jet near the cylinder at higher values of Ri (=1, 1.5) is evident from the velocity vector plots (Figures 13*a*–13*b*)

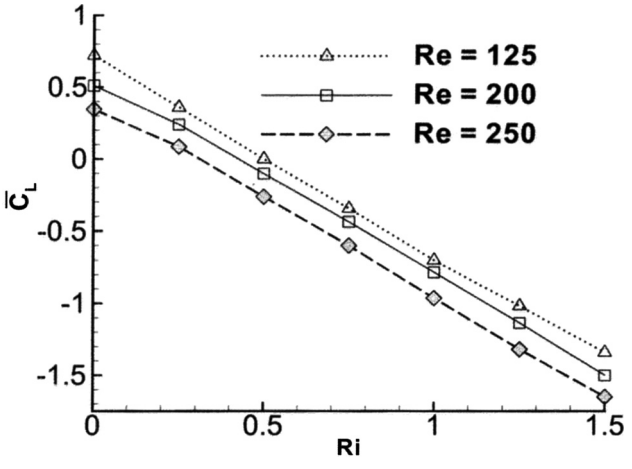

Figure 14. Variation of time-averaged lift coefficient ($\overline{C_L}$) as a function of Richardson number at Re = 125, 200, and 250.

at Re = 125. The strength of the upward jet increases with the rise of temperature of the cylinder (i.e., increase of Ri at a fixed Re).

The lift experienced by the cylinder (refer to Figure 14) is upward for lower values of Richardson number (Ri < 0.25) at all the Reynolds numbers considered, but the cylinder experiences a downward force for higher values of Richardson number. This negative lift increases monotonically with an increase of Richardson number. At higher Richardson number, the buoyancy induces a stronger negative vortex along the upper face of the cylinder, which leads to a lift directed from the higher-velocity side to the lower-velocity side of the cylinder.

The effects of heat input to the cylinder on the time-averaged surface pressure distribution at various Richardson and Reynolds numbers are shown in Figures 15*a*–15*b*. As fluid enters the gap, it encounters an adverse pressure gradient. The magnitude of the adverse pressure gradient increases with increase of the temperature of the cylinder surface at lower Re. However, the change in pressure distribution at

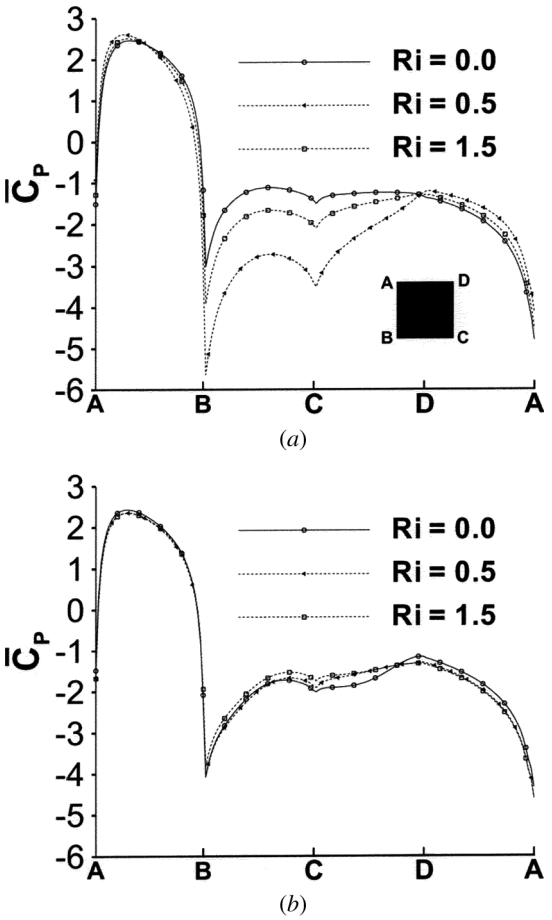

Figure 15. Time-averaged pressure distribution ($\overline{C_p}$) on the faces of the cylinder at (*a*) Re = 125 and (*b*) Re = 250 as a function of Richardson number.

Re = 250 with Ri is not prominent compared to the case of Re = 125. The pressure difference between the upper and lower sides produces net lift acting on the cylinder.

The variation of time-averaged drag coefficient ($\overline{C}_D$) with Richardson number is shown in Figure 5 for cylinder-to-wall gap height $L = 0.5$ for various values of Reynolds number (=125, 200, and 250). The drag increases monotonically with Richardson number for all values of Reynolds number. With increase of Richardson number, the wall boundary layer becomes thinner, which leads to a substantial increment in the skin friction, while the drag due to pressure drops marginally at

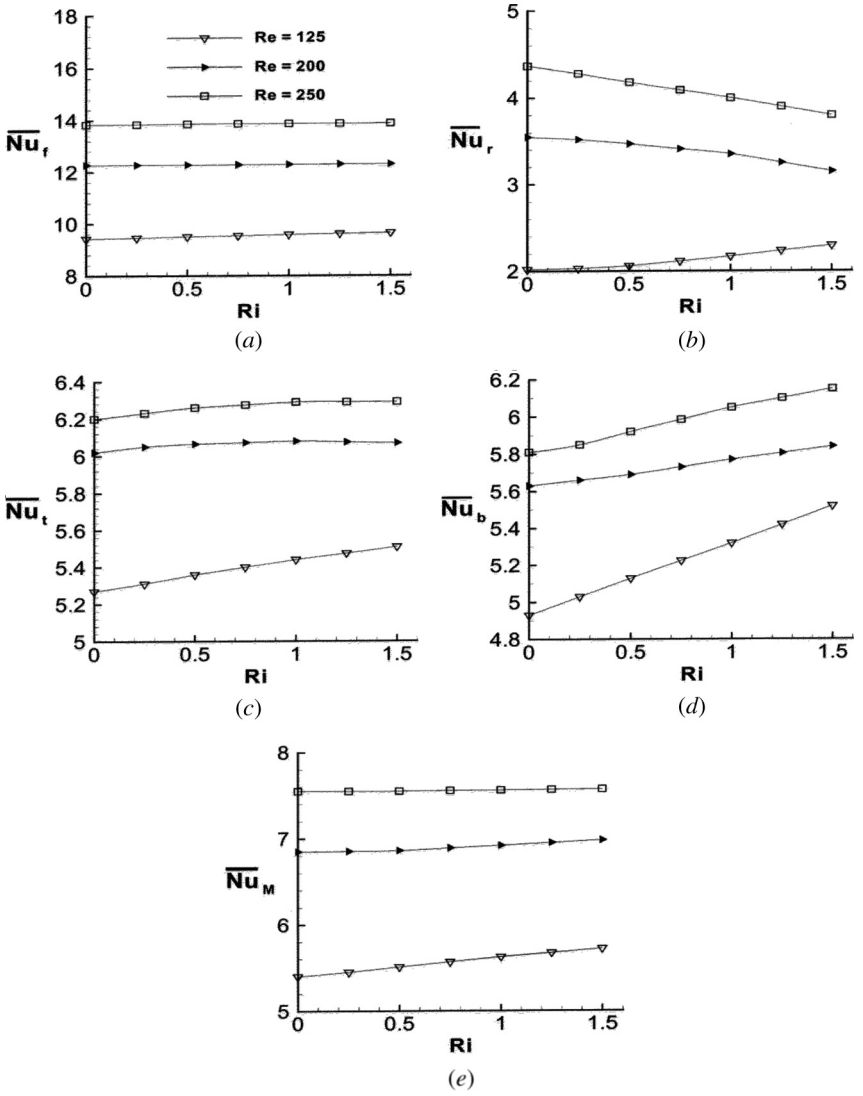

Figure 16. Effect of Richardson number on Nusselt number at the (*a*) front, (*b*) rear, (*c*) top, (*d*) bottom faces of the cylinder, and (*e*) average Nusselt number of the cylinder at Re = 125, 200, and 250. Subscripts: *f*, front; *r*, rear; *t*, top; *b*, bottom; *M*, cylinder average.

low Reynolds number. Consequently, the sum of these two components, which comprises the total drag, increases with increase of the Richardson number at the Reynolds numbers considered.

Variation of time-averaged facewise Nusselt number at four faces of the cylinder—the front, $\overline{\mathrm{Nu}}_f$, rear, $\overline{\mathrm{Nu}}_r$, top, $\overline{\mathrm{Nu}}_t$, and bottom, $\overline{\mathrm{Nu}}_b$—with Richardson number for gap height $L = 0.5$ at $\mathrm{Re} = 125$, 200, and 250 is presented in Figures 16*a*–16*d*. At low Reynolds number (=125), the heat transfer from the four faces varies linearly with Richardson number. As Richardson number increases, heat transfer from the front face increases slightly, since Richardson number has little influence on the motion of incoming fluid on the front face of the cylinder. The heat transfer from the upper and lower faces of cylinder increases monotonically with increase of Ri, due to the increment of velocity as well as the temperature difference. The heat transfer from the front face of the cylinder is much higher than the heat transfer from the other three faces of the cylinder. Along the front face, the thermal boundary layer is thinner and produces a higher heat transfer rate compared to the other faces. The rate of heat transfer along the rear face is much lower due to the recirculation of fluid close to the rear face of the cylinder.

Time-averaged Nusselt number of the cylinder ($\overline{\mathrm{Nu}}_M$) as a function of Richardson number is shown in Figure 16*e* for gap height $L = 0.5$ at $\mathrm{Re} = 125$, 200, and 250. $\overline{\mathrm{Nu}}_M$ increases with increase of Ri for fixed Re (=125, 200, and 250). The increase in Richardson number for a fixed Reynolds number implies an increase of Grashof number, which can be made by increasing the temperature difference between the cylinder surface and the ambient fluid. The rate of increment in mean Nusselt number ($\overline{\mathrm{Nu}}_M$) with increase of Richardson number is less than the corresponding rate of increment due to Reynolds number.

5. CONCLUSIONS AND FURTHER COMMENTS

The flow and heat transfer characteristics of a horizontally mounted, heated square cylinder placed within the boundary layer of a plane wall have been studied. The flow field has been analyzed for various values of Reynolds number and Grashof number with cylinder-to-wall gap height 0.5. The effect of buoyancy on the vortex shedding and the breakdown of vortex shedding have been analyzed. The major results of the present study can be highlighted as follows.

1. The onset of vortex shedding is delayed due to heating of the cylinder. Vortex shedding occurs beyond a certain critical value of the Reynolds number, which depends on Ri.
2. When the vortex shedding sets in, the shedding frequency increases with increase of Ri at a fixed Re. Our results shows that the Strouhal number St depends strongly on Re but relatively weakly on Ri. At low Reynolds number, the variation of Strouhal number, heat transfer, lift, and drag are almost linear with Ri.
3. Vortex shedding suppression can be achieved through the input of heat to the cylinder. As the surface temperature increases, a strong vertical jet sets in, which prevents the entrainment of ambient fluid penetrating into the wake cavity, and the wake consists of two oppositely rotating vortices attached to the cylinder.

Similar phenomena have been observed for the case of unbounded fluid by Kieft et al. [9].

4. Our result shows that the positive vortices in the lower row are weaker than the negative vortices shed along the upper row. The wall-induced boundary layer cancels part of the positive vorticity along the cylinder lower shear layer. The addition of heat to the cylinder further increases the difference between the positive and negative vortices. The thermally induced baroclinic vorticity production of negative signs further produces an asymmetry in the shear layers. Our finding agrees with the Kieft et al. [9] analysis for the case of a circular cylinder in an unbounded domain.
5. The time-averaged mean Nusselt numbers ($\overline{\mathrm{Nu}}_{f,r,t,b}$) at each face of the cylinder as well as the mean Nusselt number ($\overline{\mathrm{Nu}}_M$) of the cylinder are strongly dependent on Reynolds number, but the influence on $\overline{\mathrm{Nu}}_M$ due to the variation of Richardson number is not significant at large Re. As the heat transfer from the front face is the major part of total heat transfer from the cylinder, it is relatively little affected due to variation of Richardson number at large Reynolds number.

The three-dimensionality of the wake has not been addressed in the present study. Kieft et al. [28] observed through experimental analysis that the three-dimensional transition of the two-dimensional vortex street is observed for $\mathrm{Ri} > 1$. Baielly et al. [16] however, found through experimental study that the vortex shedding is more two-dimensional in the presence of a ground. We believe that the three-dimensional effect should not severely contaminate the near-wake region for the range of Reynolds number considered in this article.

REFERENCES

1. Y. M. Chung and P. G. Tucker, Numerical Studies of Heat Transfer Enhancements in Laminar Separated Flows, *Int. J. Heat Fluid Flow*, vol. 25, no. 1, pp. 22–31, 2004.
2. C. W. Leung, S. Chen, and T. L. Chan, Numerical Simulation of Laminar Forced Convection in an Air-Cooled Horizontal Printed Circuit Board Assembly, *Numer. Heat Transfer A*, vol. 37, pp. 373–393, 2000.
3. R. J. Yang and L. M. Fu, Thermal and Flow Analysis of a Heated Electronic Component, *Int. J. Heat Mass Transfer*, vol. 44, pp. 2261–2275, 2001.
4. K. Noto and R. Matsumoto, A Breakdown of the Karman Vortex Street due to the Natural Convection, *Proc. Flow Visualization III*, pp. 348–354, Springer-Verlag, Berlin, 1985.
5. K. Noto and R. Matsumoto, Numerical Simulation on the Development of the Karman Vortex Street due to the Negatively Buoyant Force, *Proc. 5th Conf. On Numerical Methods in Laminar and Turbulent Flows*, pp. 796–809, Pineridge Press, Swansea, UK, 1987.
6. K. S. Chang and J. Y. Sa, The Effect of Buoyancy on Vortex Shedding in the Near Wake of a Circular Cylinder, *J. Fluid Mech.*, vol. 220, pp. 253–260, 1990.
7. K. Hatanaka and M. Kawahara, Numerical Study of Vortex Shedding Around a Heated/Cooled Circular Cylinder by the Three-Step Taylor-Galerkin Method, *Int. J. Numer. Meth. Fluids*, vol. 21, pp. 857–867, 1995.
8. K. Noto, Computational Investigation on Wake Behavior with Buoyancy from Heated Elliptic Cylinder: Effect of Mainstream Attack Angle, *Proc. 39th Japanese Natl Congress of Applied Mechanics*, pp. 293–303, University of Tokyo Press, Tokyo, 1990.

9. R. N. Kieft, C. C. M. Rindt, A. A. Steenhoven, and G. J. F. Heijst, On the Wake Structure behind a Heated Horizontal Cylinder in Cross-Flow, *J. Fluid Mech.*, vol. 486, pp. 189–211, 2003.
10. M. Ren, C. C. M. Rindt, and A. A. van Steenhoven, Experimental and Numerical Investigation of the Vortex Formation Process behind a Heated Cylinder, *Phys. Fluids*, vol. l6, no. 8, pp. 3103–3114, 2004.
11. M. Kiya, H. Tamura, and M. Arie, Vortex Shedding from a Circular Cylinder in Moderate-Reynolds-Number Shear Flow in Cross-Flow, *J. Fluid Mech.*, vol. 101, pp. 189–211, 1980.
12. P. W. Bearmen and M. M. Zdravkovich, Flow Around a Circular Cylinder near a Plane Boundary, *J. Fluid Mech.*, vol. 89, pp. 33–47, 1978.
13. G. Bosch and W. Rodi, Simulation of Vortex Shedding past a Square Cylinder near a Wall, *Int. J. Heat Fluid Flow.*, vol. 17, pp. 267–275, 1996.
14. C. Lei, L. Cheng, and K. Kavanagh, Re-examination of the Effect of a Plane Boundary on Force and Vortex Shedding of a Circular Cylinder, *J. Wind Eng. Ind. Aerodyn.*, vol. 80, pp. 263–286, 1999.
15. L. Zovatto and G. Pedrizzetti, Flow about a Circular Cylinder between Parallel Walls, *J.Fluid Mech.*, vol. 440, pp. 1–25, 2001.
16. S. C. C. R. Bailey, R. J. Martinuzzi, and G. A. Kopp, The Effect of Wall Proximity on Vortex Shedding from a Square Cylinder: Three-Dimensional Effects, *Phys. Fluids*, vol. 14, pp. 4160–4176, 2002.
17. S. Z. Shuja, B. S. Yilbas, and M. O. Budair, Vortex Shedding Over a Rectangular Cylinder with Ground Effect: Flow and Heat Transfer Characteristics, *Int. J. Heat Fluid Flow*, vol. 12, pp. 916–939, 2001.
18. A. Sharma and V. Eswaran, Effect of Channel Confinement on the Two-Dimensional Laminar Flow and Heat Transfer across a Square Cylinder, *Numer. Heat Transfer A*, vol. 47, pp. 79–107, 2005.
19. J. L. Rosales, A. Ortega, and J. A. C. Humphrey, A Numerical Simulation of the Convective Heat Transfer in Confined Channel Flow Past Square Cylinders: Comparison of Inline and Offset Tandem Pairs, *Int. J. Heat Mass Transfer*, vol. 44, pp. 587–603, 2001.
20. H. M. Badr, Laminar Combined Convection from a Horizontal Cylinder—Parallel and Contra Flow Regimes, *Int. J. Heat Mass Transfer*, vol. 27, pp. 15–27, 1984.
21. A. A. Steenhoven and C. C. M. Rindt, Flow Transition behind a Heated Cylinder, *Int. J. Heat Fluid Flow*, vol. 24, pp. 322–333, 2003.
22. B. P. Leonard, A Stable and Accurate Convective Modeling Procedure Based on Quadratic Upstream Interpolation, *Comput. Meth. Appl. Mech. Eng.*, vol. 19, pp. 59–98, 1979.
23. R. W. Davis and E. F. Moore, A Numerical Study of Vortex Shedding from Rectangles, *J.Fluid Mech.*, vol. 116, pp. 475–506, 1982.
24. R. Franke, W. Rodi, and B. Schonung, Numerical Calculation of Laminar Vortex Shedding Flow Past Cylinders, *J. Wind Eng. Ind. Aerodyn.*, vol. 35, pp. 237–257, 1990.
25. M. P. Arnal, D. J. Georing, and J. A. C. Humphrey, Vortex Shedding from a Bluff Body Adjacent to a Plane Sliding Wall, *J. Fluids Eng.*, vol. 113, pp. 384–398, 1991.
26. R. R. Hwang and C. Yao, A Numerical Study of Vortex Shedding from a Square Cylinder with Ground Effect, *J. Fluid Eng.*, vol. 119, pp. 512–518, 1997.
27. J. H. Gerrard, The Mechanics of the Vortex Formation Region of Vortices Behind Bluff Bodies, *J. Fluid Mech.*, vol. 25, pp. 401–413, 1966.
28. R. N. Kieft, C. C. M. Rindt, and A. A. Steenhoven, Heat Induced Transition of a Stable Vortex Street, *Int. J. Heat Mass Transfer*, vol. 45, pp. 2739–2753, 2002.